Packing of crystalline structures of binary hard spheres: An analytical approach and application to amorphization

H. J. H. Brouwers
Faculty of Engineering Technology, University of Twente, P.O. Box 217, 7500 AE Enschede, The Netherlands
(Received 12 April 2007; revised manuscript received 4 June 2007; published 24 October 2007)

The geometrical stability of the three lattices of the cubic crystal system, viz. face-centered cubic (fcc), body-centered cubic (bcc), and simple cubic (sc), consisting of bimodal discrete hard spheres, and the transition to amorphous packing is studied. First, the random close packing (rcp) fraction of binary mixtures of amorphously packed spheres is recapitulated. Next, the packing of a binary mixture of hard spheres in randomly disordered cubic structures is analyzed, resulting in original analytical expressions for the unit cell volume and the packing fraction, and which are also valid for the other five crystal systems. The bimodal fcc lattice parameter appears to be in close agreement with empirical hard sphere data from literature, and this parameter could be used to distinguish the size mismatch effect from all other effects in distorted binary lattices of materials. Here, as a first model application, bimodal amorphous and crystalline fcc/bcc packing fractions are combined, yielding the optimum packing configuration, which depends on mixture composition and diameter ratio only. Maps of the closest packing mode are established and applied to colloidal mixtures of polydisperse spheres and to binary alloys of bcc, fcc, and hcp metals. The extensive comparison between the analytical expressions derived here and the published numerical and empirical data yields good agreement. Hence, it is seen that basic space-filling theories on "simple" noninteracting hard spheres are a valuable tool for the study of crystalline materials.

DOI: 10.1103/PhysRevE.76.041304 PACS number(s): 45.70.−n, 71.55.Jv

I. INTRODUCTION

Mixtures of hard spheres serve as first approximation to systems with more realistic modes of interaction. It is, for instance, known that collections of hard spheres serve as a model for the structure of simple monatomic liquids (Hansen and McDonald [1]). Also in the simple modeling of metals and alloys, the concept of hard spheres is employed to understand the formation of interstitial and substitutional alloys.

Parthé [2] used the concept of space filling to explain long-range-ordered crystalline structures. Hume-Rothery *et al.* [3] introduced the concept of favorable and unfavorable atomic size factors for the formation of solid solutions in metallic systems. Darken and Gurry [4], Chelikowsky [5], Miedema *et al.* [6], and Rauschenbach and Hohmuth [7] developed solubility maps based on both atomic size ratio and electronic properties of the constituents. Egami and Waseda [8], Liou and Chien [9], and Senkov and Miracle [10] demonstrated that both atomic size ratio and atomic concentration are the most important factors in the determination whether a regular solid solution (a disordered lattice) or a glassy and/or amorphous alloy is formed. They also derived semiempirical equations for assessing the state of the mixture (crystalline or amorphous), valid in the vicinity of either the large or the small component dominating the mixture (with a small addition of the other constituent). Also upon the crystallization of colloidal spheres, polydispersity and concentration affect the transition from a dense fluidlike structure to a crystalline structure (Luck *et al.* [11] and Pusey and Van Megen [12]). All these processes confirm the dependence on both concentration and size ratio, which is an indication that packing plays an important role in the process of amorphization. It is namely known that the void fraction of amorphously packed bimodal spheres also depends on size ratio and the concentration of the two constituents (Furnas [13], Mangelsdorf and Washington [14], and Brouwers [15]).

Accordingly, here a theoretical study is presented on the formation of binary amorphous and/or crystalline mixtures, using perfectly hard sphere models. The study is completely based on geometrical considerations, so without reference to external fields, frictional contact forces, sphere compression, or temperature. First, the packing of randomly close packed (rcp) binary spheres in the limit of small diameter ratios is recapitulated, based on recent work [15]. For rcp, the packing fraction increases with increasing diameter ratio and with concentrations that approach 50%. Next, the packing fraction of compositionally disordered binary cubic structures [viz. face-centered cubic (fcc), body-centered cubic (bcc), and simple cubic (sc)] consisting of hard spheres is analyzed. In contrast to their monosized packing fraction, which are well-known to physicist and mathematicians, expressions for the bimodal packing fractions of these cubic structures are nonexistent, with the exception of a few approximate solutions for the large sphere rich side of the composition. Also for these crystalline structures the packing fraction as an analytical function of size ratio and for the entire compositional range is derived.

For the monosized system (solely large or small spheres) the fcc structure represents the closest mode of packing, namely, $f_1^{\mathrm{fcc}}=2^{1/2}\pi/6\approx 0.74$ (here f_1 is monosized packing fraction). The bcc and sc regular packing have packing fraction $f_1^{\mathrm{bcc}}=3^{1/2}\pi/8\approx 0.68$ and $f_1^{\mathrm{sc}}=\pi/6\approx 0.52$, respectively. For rcp of monosized spheres the packing fraction f_1^{rcp} amounts to about 0.64 [16], i.e., 86% of the fcc packing fraction. But for the crystalline structures, in contrast to rcp, the mixing of two sizes results in a *reduction* of packing fraction, caused by the expansion of the lattice parameter and

TABLE I. Empirical and theoretical data on φ_1 and β for various types of particle shapes and packings, listed in [15], and based on [13,15,18,19,43–46], and the values of crystalline packing as computed here.

Material	Packing	Shape	$\varphi_1(=1-f_1)$	β	$\beta(1-\varphi_1)$
Steel[a]	rcp	spherical	0.375	0.140	0.0875
Simulation[b]	rcp	spherical	0.360	0.204	0.1306
Steel[c]	rlp	spherical	0.500	0.125	0.0625
Plastic[d]	rcp	cubical	0.433	0.134	0.0760
Quartz[e]	rcp	fairly angular	0.497	0.374	0.1881
Feldspar[e]	rcp	plate-shaped	0.503	0.374	0.1859
Dolomite[e]	rcp	fairly rounded	0.505	0.347	0.1718
Sillimanite[e]	rcp	distinctly angular	0.531	0.395	0.1853
Flint[f]	rlp	angular	0.55	0.160	0.072
Model	fcc and/or hcp	spherical	$1-2^{1/2}\pi/6$	$-21/[32(1-2^{1/2}\pi/6)]$	−1.872
Model	bcc	spherical	$1-3^{1/2}\pi/8$	$-31/[64(1-3^{1/2}\pi/8)]$	−1.030
Model	sc	spherical	$1-\pi/6$	$-381/[1024(1-\pi/6)]$	−0.409

[a]Reference [19].
[b]Reference [18].
[c]Reference [13].
[d]References [43,44].
[e]Reference [45].
[f]References [15,46].

unit cell. In this paper it will therefore also be demonstrated and quantified that the reduction (crystalline) and the increase (rcp) in packing fraction can be such that the packing fraction of both systems cross, i.e. from a topological point of view the random (amorphous) state becomes more favorable.

Finally, the theoretical results will be applied to the two crystallization processes addressed at the start of this Introduction. The first process concerns the crystallization of colloidal spheres, often employed to study the disorder-order transition from a amorphous and/or fluidlike structure to a crystalline structure. The other process concerns the classic problem of amorphization of quenched binary alloys of metals and metalloids, comprising a large variation on diameter ratios and composition. The present analysis will demonstrate the applicability and validity of "simple" hard sphere packing models to describe the state of the aforesaid more complicated and real solid state systems.

II. AMORPHOUS PACKING OF BINARY HARD SPHERES

In contrast to monosized amorphous (random) sphere packings, the packing of bimodal mixtures has hardly been examined. Furnas [13] and Mangelsdorf and Washington [14] seem to be the only ones who studied experimentally the void fraction of randomly packed bimodal hard spheres, which can also serve as a model for an amorphous or glassy solid phase. By studying binary mixtures of loosely packed spheres, it was concluded that the bimodal void fraction, h_{rcp}, depends on diameter ratio u (d_L/d_S) of large and small spheres, and on the fraction of large and small spheres. For $u\to 1$, it appeared that for optimum packing the volume and/or mole fractions of both size groups need to become equal [13,14,17]. For $u\to\infty$, ultimately, the saturated state is attained for which h_{rcp} equals $(\varphi_1^{\mathrm{rcp}})^2$ (φ_1^{rcp} being the monosized void fraction), with a pertaining volume concentration of large spheres, c_L, that amounts to $(1+\varphi_1^{\mathrm{rcp}})^{-1}$, which is larger than the volume fraction of the small spheres, c_S, that is $1-c_L$ [13].

Mangelsdorf and Washington [14] examined the packing behavior of bimodal mixes in the vicinity of a single-sized mix (i.e., when the two sizes tend to each other, that is, u tends to unity) in more detail. They executed close packing experiments with a number of binary mixes of spheres, whereby the spheres had relatively small diameter ratios of 1.16 to 1.6. Even with the largest diameter ratio, there was no apparent asymmetry in contraction (void fraction reduction). So, for $1\leq u\leq 1.6$, Mangelsdorf and Washington [14] described the void fraction reduction with a symmetrical curve of the form $X_L(1-X_L)$, where X_L is the mole fraction of the large spheres ($X_S=1-X_L$, X_S being the mole fraction of the small spheres). Their equation also implies that in the vicinity of equal sphere diameters (u tending to unity) maximum packing is obtained for $X_L=X_S=0.5$ [17]. Hence, in the vicinity of $u=1$, the binary packing fraction, $\eta_{\mathrm{rcp}}(u,X_L)$, corresponding to $1-h_{\mathrm{rcp}}(u,X_L)$, obeys

$$\eta_{\mathrm{rcp}}(u,X_L)=f_1^{\mathrm{rcp}}+4\beta f_1^{\mathrm{rcp}}(1-f_1^{\mathrm{rcp}})(1-X_L)X_L(u-1), \quad (1)$$

in which f_1^{rcp} is the monosized packing fraction, being equal to $1-\varphi_1^{\mathrm{rcp}}$. The factor β constitutes the gradient of the void fraction in the direction ($u=1$, $X_L=0.5$), being the maximum gradient of the void fraction, and hence also of the packing fraction. The factor β thus follows from an analysis of the transition from monosized to bimodal packing, and only depends on particle shape and mode of packing [e.g., rcp or random loose packing (rlp)] [15]. For a number of amorphous packing arrangements and particle shapes the values of φ_1 and β are summarized in Table I. Based on computer simulations by Kansal *et al.* [18], it follows for instance that $\beta\approx 0.20$ for rcp of spheres, being in line with rcp experiments by McGeary [19], see [15] for details, and that f_1^{rcp}

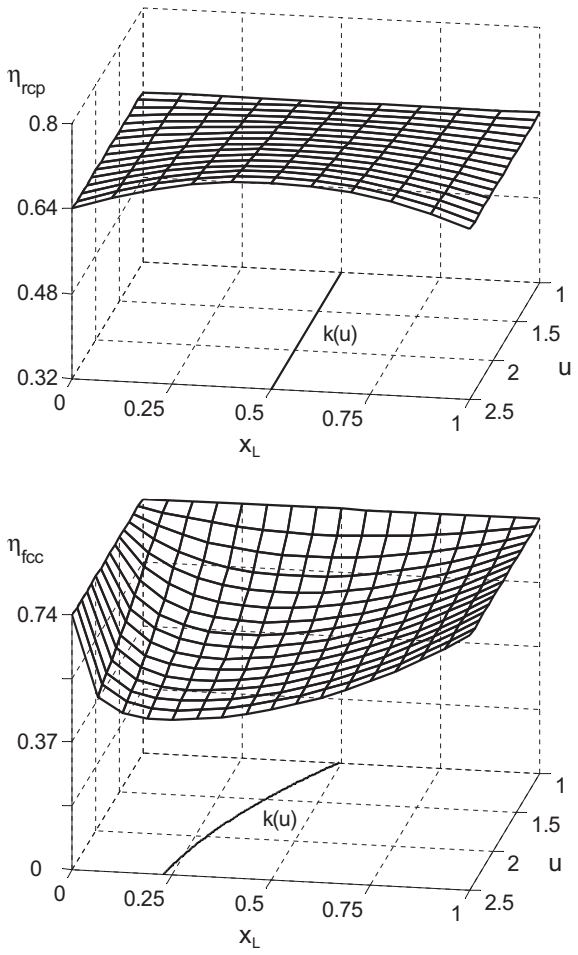

FIG. 1. (a) 3D representation of the bimodal packing fraction of rcp of spheres, η_{rcp}, as a function of size ratio u $(d_{\mathrm{L}}/d_{\mathrm{S}})$ and large sphere mole fraction X_{L}, based on Eq. (1) with $\beta=0.20$ and $f_1^{\mathrm{rcp}}=0.64$. The curve $[u, X_{\mathrm{L}}=k(u)]$, corresponding to $d\eta_{\mathrm{rcp}}/dX_{\mathrm{L}}=0$ (composition of maximum packing), is also included. (b) 3D representation of the bimodal fcc packing fraction of spheres, η_{fcc}, as a function of size ratio u $(d_{\mathrm{L}}/d_{\mathrm{S}})$ and large sphere mole fraction X_{L}, based on Eq. (21) with $n=4$ and $f_1^{\mathrm{fcc}}=0.74$. The curve $[u, X_{\mathrm{L}}=k(u)]$, corresponding to $d\eta_{\mathrm{fcc}}/dX_{\mathrm{L}}=0$ (composition of minimum packing), is also included.

≈ 0.64, this latter value also being in line with experiments [16,19] and simulations [18,20].

Alternatively, in the vicinity of $u=1$, Eq. (1) can also be approximated by

$$\eta_{\mathrm{rcp}}(u, X_{\mathrm{L}}) = f_1^{\mathrm{rcp}} + \tfrac{4}{3}\beta f_1^{\mathrm{rcp}}(1-f_1^{\mathrm{rcp}})(1-X_{\mathrm{L}})X_{\mathrm{L}}(u^3-1). \tag{2}$$

In Fig.1(a), Eq. (1) is set out in a three-dimensional (3D) graph invoking $\beta=0.20$ and $f_1^{\mathrm{rcp}}=0.64$. It follows that along $u=1$, $0\leq X_{\mathrm{L}}\leq 1$, the void and/or packing fraction retains it monosized value; physically this implies that spheres are replaced by spheres of identical size, i.e., maintaining a single-sized mixture. Also along $(u\geq 1, X_{\mathrm{L}}=0)$ and $(u\geq 1, X_{\mathrm{L}}=1)$, the packing fraction remains f_1^{rcp}, as this corresponds to the packing of unimodal spheres with diameter d_{S} and d_{L}, respectively.

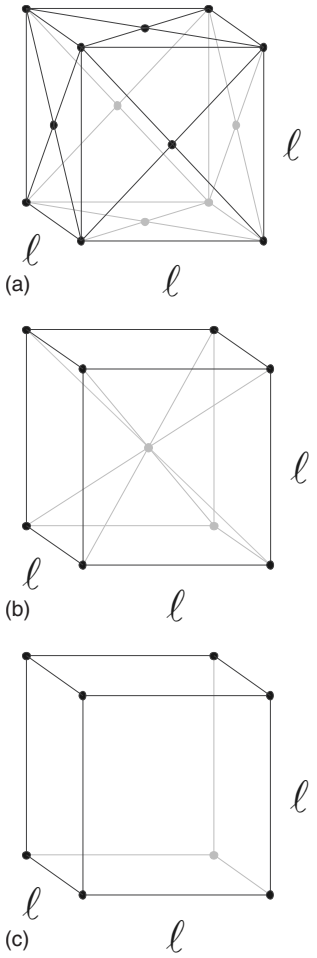

FIG. 2. Bravais lattices of cubic structures, face-centered cubic (a), body-centered cubic (b), and simple cubic (c).

As the gradient of the void fraction at $u=1$ and $X_{\mathrm{L}}=X_{\mathrm{S}}=0.5$ is zero in the direction of X_{L}, the void and/or packing fraction gradient will be largest perpendicular to this direction, i.e. in the direction of u, as discussed above. This feature of the gradient of the bimodal void fraction is also in line with the bimodal void fraction being symmetrical with respect to $X_{\mathrm{L}}=X_{\mathrm{S}}=0.5$ for u near to unity [15]. For $1<u<2.5$, i.e., the binary system, the composition at optimum packing, designated as $X_{\mathrm{L}}=k(u)$, is approximately found at $X_{\mathrm{L}}=0.5$ [Fig.1(a)] [14].

III. CRYSTALLINE STRUCTURES OF BINARY HARD SPHERES

In this section, expressions for the unit cell volume (lattice parameter) and packing fraction of crystalline cubic (face-centered cubic, body-centered cubic, and simple cubic) structures consisting of bimodal randomly placed hard spheres are derived, following a probabilistic approach, and compared with available data from literature.

For a stacking of equal spheres in a cubic structure, the packing fraction follows from the number of spheres N with diameter d in the unit cell (Fig. 2), the sphere volume Ω, and the unit cell volume V_{cell} as

$$f_1 = \frac{N\Omega}{V_{\text{cell}}} = \frac{N\frac{\pi}{6}d^3}{\ell^3}, \tag{3}$$

with ℓ as lattice constant or lattice parameter. For the fcc structure holds $N=4$ and $\ell=2^{1/2}d$, for the bcc structure $N=2$ and $\ell=2d/3^{1/2}$, and for the sc structure holds $N=1$ and $\ell=d$, yielding as monosized packing fractions $f_1^{\text{fcc}}=2^{1/2}\pi/6$, $f_1^{\text{bcc}}=3^{1/2}\pi/8$, and $f_1^{\text{sc}}=\pi/6$, respectively.

For an arrangement of bimodal spheres, the mean sphere volume readily follows as

$$\Omega = X_{\text{L}}\Omega_{\text{L}} + (1-X_{\text{L}})\Omega_{\text{S}} = \frac{\pi(X_{\text{L}}d_{\text{L}}^3 + (1-X_{\text{L}})d_{\text{S}}^3)}{6}. \tag{4}$$

The mean unit cell volume, the other key parameter that governs the packing fraction, will be analyzed in more detail in the following.

A. Cell volume

First, expressions for the unit cell volume are derived for bimodal cubic structures. For a perfectly randomly disordered bimodal fcc phase, i.e., all spheres randomly placed on the lattice sites and exhibiting no short-range order, the unit cell volume is governed by tetrahedra as the elementary building blocks. The compositional combinations of small and large spheres statistically follow as

$$V_{\text{cell}} = \sum_{i=0}^{n}\left[\binom{n}{i}X_{\text{L}}^{n-i}(1-X_{\text{L}})^i\left(\frac{n-i}{n}\ell_{\text{L}}^3 + \frac{i}{n}\ell_{\text{S}}^3 + \lambda(\ell_{\text{L}}^3 - \ell_{\text{S}}^3)\right)\right] - \lambda[X_{\text{L}}^n + (1-X_{\text{L}})^n](\ell_{\text{L}}^3 - \ell_{\text{S}}^3), \tag{5}$$

with $n=N=4$ for fcc. For the bcc structure, though the number of spheres N in a unit cell amounts to 2 only (due to repetition in case of equal spheres), minimal 6 spheres are involved in the computation of the monosized packing fraction, so then $n=6$. For the simple cubic structure holds $N=1$, but the building block that governs the cell volume contains 8 spheres, so for this lattice $n=8$ [Figs. 2(a)–2(c)].

In Eq. (5), the lattice distortion is accounted for by the factor λ, which allows for the spacing resulting from the combination of the large and small spheres in the cells in which they both appear. It is supposed to be a linear function of the volume mismatch, and the distortion tends to zero when ℓ_{S}^3 tends to ℓ_{L}^3, that is, when a monosized system is obtained and V_{cell} should tend to $\ell_{\text{S}}^3=\ell_{\text{L}}^3$. The two last terms on the right-hand side provide that the building blocks consisting of identical spheres, large or small only, are counted as nondistorted (i.e., in the state of close monosized packing). Using the binomial theorem

$$\sum_{i=0}^{n}\left[\binom{n}{i}X_{\text{L}}^{n-i}(1-X_{\text{L}})^i\right] = [X_{\text{L}} + (1-X_{\text{L}})]^n = 1, \tag{6}$$

Eq. (5) can be rewritten as

$$V_{\text{cell}} = X_{\text{L}}\ell_{\text{L}}^3 + (1-X_{\text{L}})\ell_{\text{S}}^3 + \lambda[1 - X_{\text{L}}^n - (1-X_{\text{L}})^n](\ell_{\text{L}}^3 - \ell_{\text{S}}^3). \tag{7}$$

For $\lambda=0$, i.e., no mismatch between jointly packed large and small spheres in a cell, Eq. (7) yields

$$V_{\text{cell}} = X_{\text{L}}\ell_{\text{L}}^3 + (1-X_{\text{L}})\ell_{\text{S}}^3, \tag{8}$$

and the packing fraction then would remain constant throughout the entire concentration series, see Eqs. (3), (4), and (8).

Equation (8) is a volume additive equation, observed by Retgers [21] to hold for many mixtures of salts (referred to as "Retgers' rule"), and which was also discussed later by Zen [22]. As will be seen, it is not applicable to hard sphere packing. Later, to overcome the observed discrepancy and match lattice parameters of metal solutions properly, Van Arkel and Basart [23] introduced the general power-law equation

$$\ell^q = X_{\text{L}}\ell_{\text{L}}^q + (1-X_{\text{L}})\ell_{\text{S}}^q, \tag{9}$$

which turns into Retgers' equation [Eq. (8)] for $q=3$. Van Arkel and Basart [23] applied Eq. (9) to quenched solutions of gold and copper with as best fit $q=5$. Furthermore, note that for $q=1$, a linear relation is obtained that is often attributed to Vegard [24]. This linear equation is an approximate rule only, which appeared to be valid for a number of ionic salts, but never quite true in metallic systems.

Here, for hard spheres, it is reasonable to assume that when small spheres are introduced in a structure of large spheres only, it will not change the cell volume, in other words, the small sphere will be able to rattle in its cage formed by the larger sphere volume. Mathematically, this implies that the first derivative of the cell volume with respect to X_{L},

$$\frac{dV_{\text{cell}}}{dX_{\text{L}}} = 3\ell^2\frac{d\ell}{dX_{\text{L}}} = (\ell_{\text{L}}^3 - \ell_{\text{S}}^3)\{1 - \lambda n[X_{\text{L}}^{n-1} - (1-X_{\text{L}})^{n-1}]\}, \tag{10}$$

equals zero, that is to say,

$$\left.\frac{dV_{\text{cell}}}{dX_{\text{L}}}\right|_{X_{\text{L}}=1} = 0, \tag{11}$$

yielding

$$\lambda = 1/n. \tag{12}$$

Consequently, at the small sphere rich side, the lattice gradient as given by Eqs. (10) and (12) is governed by

$$\left.\frac{dV_{\text{cell}}}{dX_{\text{L}}}\right|_{X_{\text{L}}=0} = 2(\ell_{\text{L}}^3 - \ell_{\text{S}}^3). \tag{13}$$

This derivative at $X_{\text{L}}=0$ (at which $\ell=\ell_{\text{s}}$ and $V_{\text{cell}}=\ell_{\text{s}}^3$) learns that the gradient of Eq. (7) is two times the gradient involved with the linear equation (8).

For the fcc lattice, i.e., $n=4$ and $\lambda=1/4$, see Eq. (12), according to Eq. (7) the scaled cell volume becomes

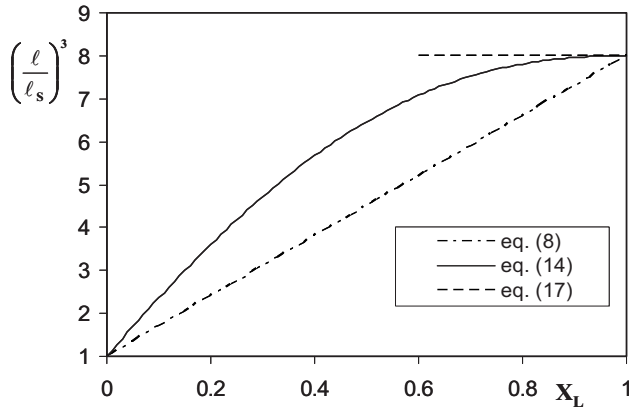

FIG. 3. Scaled cell volume of fcc packing $[(\ell/\ell_S)^3]$ following Eq. (17) [25–27], Eq. (8) [21], and this study, Eq. (14).

$$(\ell/\ell_S)^3 = X_L(u^3-1) + 1 + \tfrac{1}{4}[1 - X_L^4 - (1-X_L)^4](u^3-1), \tag{14}$$

whereby is invoked

$$u = \frac{\ell_L}{\ell_S} = \frac{d_L}{d_S}. \tag{15}$$

Jalali and Li [25] assumed a constant fcc cell volume, based on large sphere size, so

$$V_{cell} = \ell_L^3 = 2d_L^3\sqrt{2}, \tag{16}$$

or dimensionless

$$V_{cell}/\ell_S^3 = u^3. \tag{17}$$

Equations (16) and (17) imply that all small spheres have clearance to move, irrespective of their concentration. This approach, that appeared also to be proposed by Denton and Ashcroft [26] already [27,28], implies a constant lattice parameter, which is applicable only when $X_L \to 1$.

In Fig. 3, the different unit volume concepts are explained by setting out the scaled fcc cell volume $(\ell/\ell_S)^3$ against the large sphere concentration X_L for, as example, a binary mixture with size ratio $u=2$. In Fig. 3, Eq. (16) and Retgers' equation, i.e., the linear cell volume relation (8), both also scaled with ℓ_S^3, are included. The first equation implies the extreme case whereby the larger unit cell volume prevails everywhere, whereas Retger's equation ignores the nonlinear expansive effect by the mixing of small and large spheres, and can be considered as the other extreme case. Equation (14), on the other hand, yields a scaled cell volume that ranges from 1 ($X_L=0$) to u^3 ($X_L=1$) throughout the entire series of mixtures, and is located between the two former extreme cases. Fig. 3 also reveals that the lattice parameter gradient near $X_L=1$ (the large sphere rich side) is zero, and at $X_L=0$ (the small sphere rich side) two times the gradient involved with Retgers' linear equation, which is a consequence of Eqs. (10) and (11) and resulting equation (12).

Here, expressions for the binary lattice parameters are derived for the three cubic structures, and illustrated more in detail for the fcc structure. In the following section the fcc expression in particular is validated. To the author's knowledge, no such data is yet available for the bimodal bcc and sc structures, and it appears that empirical fcc data is also rather scarce. But sufficient and valuable data is found for a thorough validation.

B. Comparison with empirical lattice data

Luck *et al.* [11] executed pioneering experiments concerning the crystallization of colloids with 0.1 to 1 μm diameter. Using transmission and reflection spectra, monodisperse and bimodal lattices of crystalline packings were identified as Bragg reflexes with visible light. It was recognized that these lattices yield interesting optical parallels to structural investigations by means of x-ray diffraction (XRD). The authors reported useful results in regard to the lattice constants of four types of monosized dispersions and of their bidisperse combinations. The lattice parameters of the monosized dispersions were 375 nm, 404 nm, 414 nm, and 472 nm, designated as "L32," "L34," "L36," and "L33," respectively. The combinations of "L32" and "L34" and of "L34" and "L36" had lattice parameters that exhibited no contraction, the measured lattice parameters presented in [11] appeared even to be smaller than computed with Eq. (9) using $q=3$ (Retgers' law). This result can most probably be attributed to the small difference in lattice parameters and resulting difficulty of measuring the lattice parameter of the mix accurately. On the other hand, the mixes of "L32" and "L36" and of "L32" and "L33" exhibited the expected lattice expansion; in Table II the compositions are given and the measured bimodal lattice constant. In [11] mass and/or volume fractions of the combined dispersions are actually given (Luck [29]); they are expressed in mole fractions by

$$X_L = \frac{c_L}{c_L + (1-c_L)u^3}. \tag{18}$$

In Table II the computed mole fraction are included too, as well the computed lattice parameter using Eq. (14) and Eq. (9) with $q=3$ (Retgers' equation). One can see that Retgers' law underestimates the expansion of the lattice by mixing of

TABLE II. Lattice parameters measured by Luck *et al.* [11], and their values computed here: Eq. (14), and Eq. (9) with $q=3$ ($\ell_{Retgers}$) and with $q=1$ (ℓ_{Vegard}).

c_L	ℓ_L (nm)	ℓ_S (nm)	u	z	X_L	measured (nm)	Eq. (14) (nm)	$\ell_{Retgers}$ (nm)	ℓ_{Vegard} (nm)
0.500	414	375	1.104	2.894	0.426	403	401	393	392
0.901	472	375	1.259	1.006	0.048	385	386	381	380

the two sizes. This underestimation is even worse by Vegard's equation. Equation (14), on the other hand, predicts lattice parameters that are very close to the empirical observation. This is a remarkable result for the derivation of the binary lattice parameter is based on first principles, without any adjustable parameter.

Next, Eq. (14) is validated for a bimodal fcc structure with small size ratio, using experimental data from Steinwehr [30]. In [30] hard spheres with a size ratio $u=1.06$ are packed. The absolute sizes were not specified, but from a photo ("Fig. 1") one can see that the sizes were most likely of order mm. The small and large spheres were packed hexagonally on a flat plate, on which they were randomly placed in equal numbers ($X_L=0.5$). Steinwehr [30] related the mean lattice parameter to a computed lattice parameter based on the linear rule [Eq. (9) with $q=1$]. Compared to the linear lattice equation, a relative expansion (dilatation), designated as "q" [30], of about 1% was measured. Using Eq. (9), with $q=1$, and Eq. (14), this property "q" corresponds to

$$\frac{\ell}{\ell_{\text{Vegard}}} - 1 = \frac{\left\{X_L(u^3-1)+1+\frac{1}{4}(1-X_L^4-(1-X_L)^4)(u^3-1)\right\}^{1/3}}{X_L(u-1)+1} - 1. \tag{19}$$

Substituting the corresponding values of Steinwehr [30], $u=1.06$ and $X_L=0.5$, in this equation yields a relative expansion value of 1.3%. This value, obtained with the present packing model, is quite close to the aforesaid "q" value of 1%, particularly when the explorative purpose of this single experiment is considered.

In Eq. (19), the lattice parameter is derived from the mean cell volume by taking its cubic root. The linear approximation of the lattice parameter becomes apparent when the cell volume, Eq. (14), is asymptotically expanded for small $u-1$

$$(\ell/\ell_S) = X_L(u-1)+1+\tfrac{1}{4}[1-X_L^4-(1-X_L)^4](u-1). \tag{20}$$

The first two terms on the right-hand side now feature the linear part of the relation between the scaled lattice constant of the packing and the concentrations of the two constituents (Vegard's equation). Here, it is seen from Eq. (20) that this linear part is not sufficient to describe a binary hard sphere fcc structure, and neither for the other crystalline hard sphere structures, due to the third and nonlinear term on the right-hand side, that features in all bimodal crystalline packing equations (previous section). Note that the lattice parameter approximation, Eq. (20), can be derived from the mean cell volume, but that the mean cell volume in turn does not follow from taking the third power of this mean lattice parameter (approximation).

Hence, the thorough comparison with empirical data yields the conclusion that Eq. (14), constituting the fcc cell volume as derived in the previous section, provides reliable results, to say the least. Note that this equation is solely based on first principles, and no fitting parameter is introduced nor required. Together with Eq. (4), this cell volume thus provides a compact and useful expression for the packing fraction of the bimodal fcc structure.

C. Binary packing fraction of crystalline structures

The information on mean sphere volume and cell volume can be combined in order to obtain the packing fraction. Using Eq. (15), and substituting Eqs. (4) and (7) in Eq. (3), yields a general scaled bimodal packing fraction of the cubic structures,

$$\frac{\eta}{f_1} = \frac{X_L(u^3-1)+1}{X_L(u^3-1)+1+\frac{1}{n}[1-X_L^n-(1-X_L)^n](u^3-1)}. \tag{21}$$

Equation (21) correctly predicts that the packing tends to the monosized value for both $X_L=0$ (small spheres only) and $X_L=1$ (large spheres only), and is valid in the entire compositional range. This feature of the present model follows from the fact that for a group of n small spheres the probability is introduced that they may pack as closely as in a monosized mix. Equation (21) also readily reveals that for $0<X_L<1$, $\eta/f_1<1$, which is caused by the third term in the denominator, which is the mismatch or distortion term. Whereas for rcp the packing fraction increases by combining bimodal spheres [Fig. 1(a)], in a disordered crystal lattice the packing fraction is reduced by lattice expansion, caused by the topological disorder.

For purposes of the present analysis, the bimodal packing equation is also linearized to the case of u close to unity. For small (u^3-1), Eq. (21) can be asymptotically approximated by

$$\frac{\eta}{f_1} = 1 - \frac{1}{n}[1-X_L^n-(1-X_L)^n](u^3-1) + O[(u^3-1)^2]. \tag{22}$$

In contrast to the original Eq. (21), Eq. (22) facilitates the application of the bimodal packing model and it enables an analytical approximate solution of the system that will be studied in the following section.

Equations (21) and (22) also yields the gradient β, introduced in [15], and also used in Sec. II,

$$\beta = -\frac{1}{\varphi_1(1-\varphi_1)}\left.\frac{dh}{du}\right|_{u=1,X_L=0.5} = \frac{1}{f_1(1-f_1)}\left.\frac{d\eta}{du}\right|_{u=1,X_L=0.5} = \frac{-3\left[1-\left(\frac{1}{2}\right)^{n-1}\right]}{(1-f_1)}, \tag{23}$$

amounting $-21/[32(1-f_1^{\text{fcc}})]$ for fcc ($n=4$), $-31/[64(1-f_1^{\text{bcc}})]$ for bcc ($n=6$), and $-381/[1024(1-f_1^{\text{sc}})]$ for sc ($n=8$). These negative values of β, illustrating the packing decrease, are included in Table I.

For fcc, i.e., $n=4$, Eq. (21) becomes

$$\frac{\eta_{\mathrm{fcc}}}{f_1^{\mathrm{fcc}}} = \frac{X_L(u^3-1)+1}{X_L(u^3-1)+1+\frac{1}{4}(1-X_L^4-(1-X_L)^4)(u^3-1)} = \frac{X_L(u^3-1)+1}{X_L(u^3-1)+1+(1-X_L)X_L\left[1-\frac{1}{2}(1-X_L)X_L\right](u^3-1)}. \tag{24}$$

In Fig. 1(b), Eq. (24) is set out in a 3D graph for $n=4$ (fcc) and using $f_1^{\mathrm{fcc}}=0.74$. Figures 1(a) and 1(b) clearly illustrate that the rcp packing achieves a higher packing fraction upon mixing two sizes, whereas the fcc packing fraction decreases. The asymptotic approximation for small (u^3-1) of Eq. (24) reads

$$\frac{\eta_{\mathrm{fcc}}}{f_1^{\mathrm{fcc}}} = 1-(1-X_L)X_L\left[1-\frac{1}{2}(1-X_L)X_L\right](u^3-1) + O[(u^3-1)^2], \tag{25}$$

which also corresponds to Eq. (22) when $n=4$ is invoked. In Fig. 4(a), $\eta_{\mathrm{fcc}}/f_1^{\mathrm{fcc}}$ is set out for $u=1.2$ and $u=2.4$ versus the large component concentration (X_L) using Eq. (24). From a structural point of view it follows that Eq. (24) also hold for the bimodal hexagonal close packing (hcp), that is to say, they are the same as for the fcc packing. Though the number of spheres of a unit cell is 6 instead of 4, also in hexagonal packing the smallest unit is a tetrahedron and the number of spheres involved again amounts to 4. These are the 4 spheres that, likewise in the fcc structure, form tetrahedra. As the derivation of Eq. (21) is based on the deviation from the monosized sphere volume and the monosized lattice parameter, resulting in a function scaled by the monosized packing fraction, for $n=4$ it can also be used for face-centered orthorhombic structures, for which the packing fraction is also governed by building blocks of 4 spheres.

The bimodal packing fraction of the bcc structure follows from Eq. (21) and substituting $n=6$, which is set out for $u=1.2$ and $u=2.4$ versus the large component concentration in Fig. 4(b). One can see that the relative reduction in packing of the bcc structure is smaller than for an fcc structure under equal conditions (concentration and size ratio), which is due to the relatively smaller expansion of the cell volume.

The bimodal bcc packing equation, i.e., Eq. (21) with $n=6$, can be satisfactory approximated by

$$\frac{\eta_{\mathrm{bcc}}}{f_1^{\mathrm{bcc}}} = \frac{X_L(u^3-1)+1}{X_L(u^3-1)+1+(1-X_L)X_L\left[1-\frac{3}{2}(1-X_L)X_L\right](u^3-1)}, \tag{26}$$

as can be seen in Fig. 4(b). The asymptotic approximation for small (u^3-1) of Eq. (26) reads

$$\frac{\eta_{\mathrm{bcc}}}{f_1^{\mathrm{bcc}}} = 1-(1-X_L)X_L\left[1-\frac{3}{2}(1-X_L)X_L\right](u^3-1) + O[(u^3-1)^2]. \tag{27}$$

The right-hand sides of Eq. (21) with $n=6$, and of Eqs. (26) and (27) will also hold for body-centered orthorhombic and tetragonal structures, and for base-centered monoclinic and orthorhombic structures.

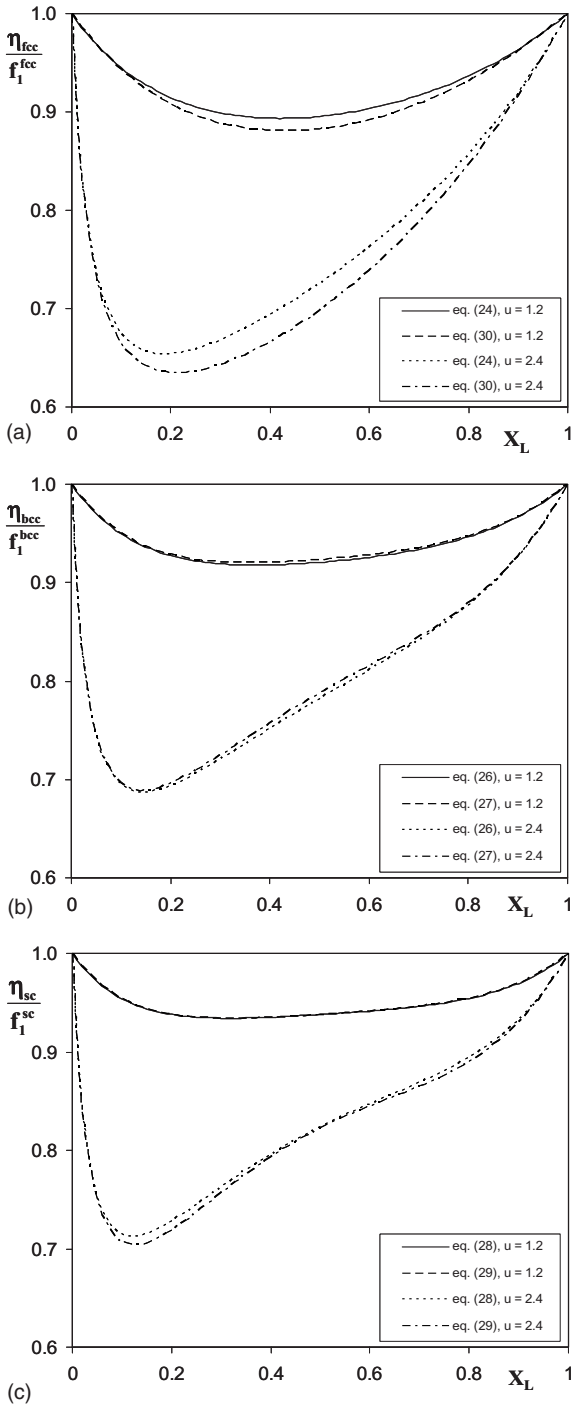

FIG. 4. (a) Scaled packing fraction of the bimodal fcc ($\eta_{\mathrm{fcc}}/f_1^{\mathrm{fcc}}$) structure for $u=1.2$ and $u=2.4$ in the range $0\leq X_L\leq 1$. (b) Scaled packing fraction of the bimodal bcc ($\eta_{\mathrm{bcc}}/f_1^{\mathrm{bcc}}$) structure for $u=1.2$ and $u=2.4$ in the range $0\leq X_L\leq 1$. (c) Scaled packing fraction of the bimodal sc ($\eta_{\mathrm{sc}}/f_1^{\mathrm{sc}}$) structure for $u=1.2$ and $u=2.4$ in the range $0\leq X_L\leq 1$.

The bimodal sc packing fraction is governed by Eq. (21) with $n=8$, which can be approximated by

$$\frac{\eta_{sc}}{f_1^{sc}} = \frac{X_L(u^3-1)+1}{X_L(u^3-1)+1+(1-X_L)X_L[1-2(1-X_L)X_L](u^3-1)}. \tag{28}$$

In Fig. 4(c), Eq. (21) with $n=8$ and Eq. (28) are set out. Equation (28) is asymptotically approximated for small (u^3-1) by

$$\frac{\eta_{sc}}{f_1^{sc}} = 1-(1-X_L)X_L[1-2(1-X_L)X_L](u^3-1) + O[(u^3-1)^2]. \tag{29}$$

The monosized sc packing fraction is lower than those of the bcc and fcc structures, and even lower than rcp. But the effect of combining two spheres sizes has less effect on the packing fraction than is the case for fcc and bcc, compare Figs. 4(a)–4(c). Note that in Fig. 4(c) the relative packing curve for $u=1.2$ and 2.4 are given, to permit comparison with Figs. 4(a) and 4(b), but that actually sc interstitial packing is already feasible at a size ratio u of $(\sqrt{3}-1)^{-1}$, which is to say, $u\approx 1.37$. The right-hand sides of Eq. (21) with $n=8$, and of Eqs. (28) and (29) will also be valid, due to structural similarity, for triclinic structures, for simple monoclinic, orthorhombic and tetragonal structures, and for rhombohedral (trigonal) structures.

All scaled (relative) packing functions [Figs. 4(a)–4(c)] illustrate that the absolute reduction of a crystalline packing is linearly dependent on the monosized packing fraction of such packing. From the bimodal crystalline hard sphere packing analysis it is furthermore seen that, whereas for rcp the packing fraction increases by combining bimodal spheres (Sec. II), these disordered lattices have a reduced packing fraction by lattice expansion. The packing equations furthermore confirm the symmetrical (with respect to equisphere compound $X_L=X_S=0.5$) behavior for u tending to unity. The same characteristics were observed for the amorphous packing of hard spheres (Sec. II). For equal diameter ratio u $(u>1)$, the bimodal crystalline packings exhibit a larger expansion than the amorphous packing that undergoes contraction. This is also illustrated by the difference in magnitude of β (Table I). The packing equations also reveal that the packing fraction near $u=1$ is linearly dependent on u^3-1 (or $u-1$), analogous to the amorphous packing (Sec. II), which is a consequence of the assumed mismatch mechanism and its linear disorder terms. Packing models based on the Percus-Yevick (PY) equation, on the other hand, yield a system contraction and/or expansion proportional to $(u^3-1)^2$ or $(u-1)^2$ [15]. The gradient of the packing fraction is then predicted to be zero at $u=1$, which is questionable. This PY equation originates from the compressibility theory of fluids, and seems to be applicable to model hard sphere systems only when the packing density is not close to its maximum.

One can furthermore observe in Fig. 1(b) and Figs. 4(a)–4(c) that for crystalline packings the maximum void fraction for $u>1$ is found at $X_L<0.5$, and that this eccentricity is pronounced. For amorphous packings, on the other hand, maximum packing is found at $X_L>0.5$, which becomes noticeable only for larger size ratios [15].

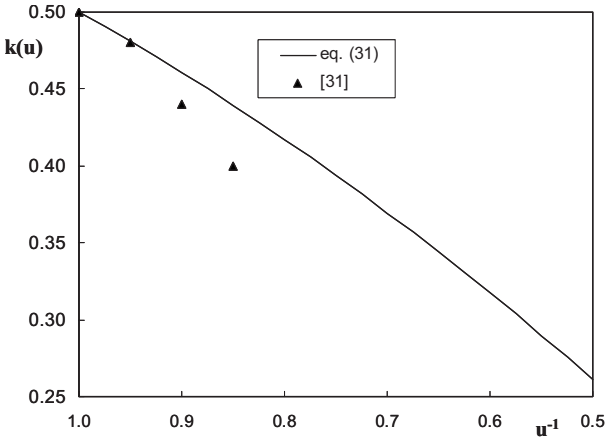

FIG. 5. Concentration of large spheres as a function of the inverse size ratio (u^{-1}) at minimum packing fraction $[X_L=k(u)]$ for a bimodal fcc structure, using data from [31] and Eq. (31).

D. Comparison with packing data

The combined Monte Carlo and molecular dynamics simulations of hard spheres by Kranendonk and Frenkel [31] provide some results that can be used indicatively, as these simulations did not concern systems at closest packing, as is addressed here. An absolute comparison between packing fractions can therefore not be made, but their computed reduced pressure at constant packing density can be used for a qualitative comparison. These reduced pressures reveal that the composition at minimum packing fraction is found for $X_L<0.5$, being in line with the present findings. In Fig. 5 their X_L at minimum packing, denoted by $k(u)$, are set out against u^{-1}.

To derive analytical expression for the composition X_L at minimum packing, first Eq. (21) with $n=4$, is approximated by

$$\frac{\eta_{fcc}}{f_1^{fcc}} = \frac{X_L(u^3-1)+1}{X_L(u^3-1)+1+(1-X_L)X_L(u^3-1)}. \tag{30}$$

In Fig. 4(a), Eq. (30) is set out and it appears that it is a good approximation of Eq. (24) indeed. Differentiating Eq. (30) with respect to X_L and equating this derivative with zero results in the following explicit expression:

$$k(u) = \frac{u^{3/2}}{u^{3/2}+1}. \tag{31}$$

This equation is included in Fig. 5 as well, and a reasonable agreement can be observed with the computational data [31]. Though the underlying models and considered systems are different, the trends are very alike.

In this section it is quantitatively and qualitatively confirmed that the models for closely packed bimodal cubic structures provide useful expressions for cell volume and lattice parameter, as well as the bimodal crystalline packing fraction. They can, for example, also be used for the further assessments on the state of hard spheres mixtures and metal and/or metalloid alloys. When metal or metalloids are alloyed, the effective lattice parameter is namely the result of geometrical dilatation and other effects, such electronic con-

traction. If the actual lattice parameter or distortion parameter of the alloy is specified, which are actually measured already for many binary crystalline substances, the present equations for the geometrical expansion enable the quantification of all other effects.

In the next section the expressions will be used to study the stability of the crystalline packings and their crossover to amorphous packing, and the resulting diagrams of closest packing are applied to real systems.

IV. THRESHOLD CRYSTALLINE AND/OR AMORPHOUS PACKING

In the previous sections the packing fractions of bimodal rcp and of bimodal crystalline structures were presented. The random amorphous packing features an increased packing fraction on combining two sphere sizes, whereas the random crystalline packing exhibits reduced packing. These opposite effects of mixing, and their effect on the topological stability of the crystalline packing, will be employed and discussed in more detail in the present section. To this end, the packing fractions will be computed and their intersection, in particular the crossover from either fcc or bcc to rcp, determined. In this way two diagrams of closest packing, distinguishing crystalline, and amorphous arrangements, are established.

A. Fcc stability

In Fig. 6(a), η_{rcp} and η_{fcc} are set out, following Eq. (1) using $f_1^{\mathrm{rcp}}=0.64$ and $\beta=0.20$, and Eq. (21) using $n=4$ and $f_1^{\mathrm{fcc}}=0.74$, respectively, for $u=1.234$ and X_{L} ranging from 0 to 1. One can readily recognize the monosized packing fractions of both packing modes at $X_{\mathrm{L}}=0$ (small spheres only) and $X_{\mathrm{L}}=1$ (large spheres only), being 0.74 and 0.64, respectively. The figure also illustrates once more the contraction and expansion of the amorphous and/or glass and crystalline packing, respectively, as a result of combining two sphere sizes. This change in packing is most pronounced when the concentration of the two components is close to parity (X_{L} close to 0.5), and the largest change in packing fraction occurs within the fcc structure. The selected size ratio u is such that there is a composition whereby the crystalline and amorphous packing fractions are the same. But in the entire compositional range ($0\leq X_{\mathrm{L}}\leq 1$) the fcc arrangement still has highest space filling ability. Now, the central idea is that from a topological point of view, namely a stable packing, hard spheres (and atoms) preferably organize into this arrangement.

In Fig. 6(b) also amorphous and cubic close packing fractions for $u=1.35$ are depicted. Now it can be seen that the change in packing fractions is such that there is a compositional range where the binary rcp packing fraction exceeds the fcc packing fraction. This scenario of highest packing is indicated by the solid line, which indicates the mechanically stable situation of highest packing efficiency. Below $X_{\mathrm{L,min}}$ and above $X_{\mathrm{L,max}}$, fcc is still most preferable, but at intermediate compositions, the mixture becomes more stable if it collapses into a glass and/or amorphous state. Apparently, this signals there are compositional regions, depending on the size ratio u, where either a fcc or a rcp phase is uniquely favored.

To specify the crossover boundary between crystal to glass phase, Eqs. (1) and (21) are equated ($n=4$), yielding an implicit equation in u and X_{L}:

$$f_1^{\mathrm{rcp}}+4\beta f_1^{\mathrm{rcp}}(1-f_1^{\mathrm{rcp}})(1-X_{\mathrm{L}})X_{\mathrm{L}}\left(\frac{(z+1)^{1/3}-z^{1/3}}{z^{1/3}}\right)$$
$$=f_1^{\mathrm{fcc}}\left(\frac{z+X_{\mathrm{L}}}{z+X_{\mathrm{L}}+1+\frac{1}{4}[1-X_{\mathrm{L}}^4-(1-X_{\mathrm{L}})^4]}\right), \qquad (32)$$

in which is introduced

$$z=\frac{\Omega_{\mathrm{S}}}{\Omega_{\mathrm{L}}-\Omega_{\mathrm{S}}}=\frac{1}{u^3-1};\quad u-1=\frac{(z+1)^{1/3}-z^{1/3}}{z^{1/3}}. \qquad (33)$$

In Fig. 6(c) the solution of Eq. (32) is given, whereby the crossover z is set out against X_{L}. The equilibrium line is actually the result of the intersection of the two curves set out in Fig. 1. This equilibrium line represents the threshold of densest packing between rcp and fcc. For z exceeding this equilibrium, i.e., a smaller size ratio, fcc yields densest packing, below this line rcp yields the densest packing fraction. Note that the maximum threshold value of z, $z\approx 1.138$, corresponds to a minimum $u=1.234$, being the value of z above which (value of u below which) a fcc lattice always yields a highest packing fraction, as was seen in Fig. 6(a). Hence, binary spheres with smaller size ratio u may form continuous series of crystalline solid solutions.

For u close to unity, approximate Eqs. (2) and (24) can be equated and combined with Eq. (33), yielding the explicit equation

$$z=(1-X_{\mathrm{L}})X_{\mathrm{L}}\left(\frac{\frac{4}{3}\beta f_1^{\mathrm{rcp}}(1-f_1^{\mathrm{rcp}})+f_1^{\mathrm{fcc}}\left[1-\frac{1}{2}(1-X_{\mathrm{L}})X_{\mathrm{L}}\right]}{f_1^{\mathrm{fcc}}-f_1^{\mathrm{rcp}}}\right), \qquad (34)$$

which is also included in Fig. 6(c). One can see that this approximate equation matches the full equation reasonably well.

B. bcc stability

Next, in Fig. 7(a), η_{rcp} and η_{bcc} are set out, following Eq. (1), using $f_1^{\mathrm{rcp}}=0.64$ and $\beta=0.20$, and Eq. (21), using $n=6$ and $f_1^{\mathrm{bcc}}=0.68$, for $u=1.117$ and X_{L} ranging from 0 to 1. One can readily recognize the monosized packing fractions of both packing modes at $X_{\mathrm{L}}=0$ (small spheres only) and $X_{\mathrm{L}}=1$ (large spheres only), being 0.68 and 0.64, respectively. The figure also illustrates the contraction and expansion of the amorphous/glass and crystalline packing, respectively, as a result of combining two sphere sizes. This change in packing is most pronounced when the concentration of the two components is close to 50% (X_{L} close to 0.5), and the bcc structure exhibits the largest change in packing fraction (compared to rcp). The selected size ratio u is such that at this composition of equal concentration the packing fractions are the same. For in the entire compositional range

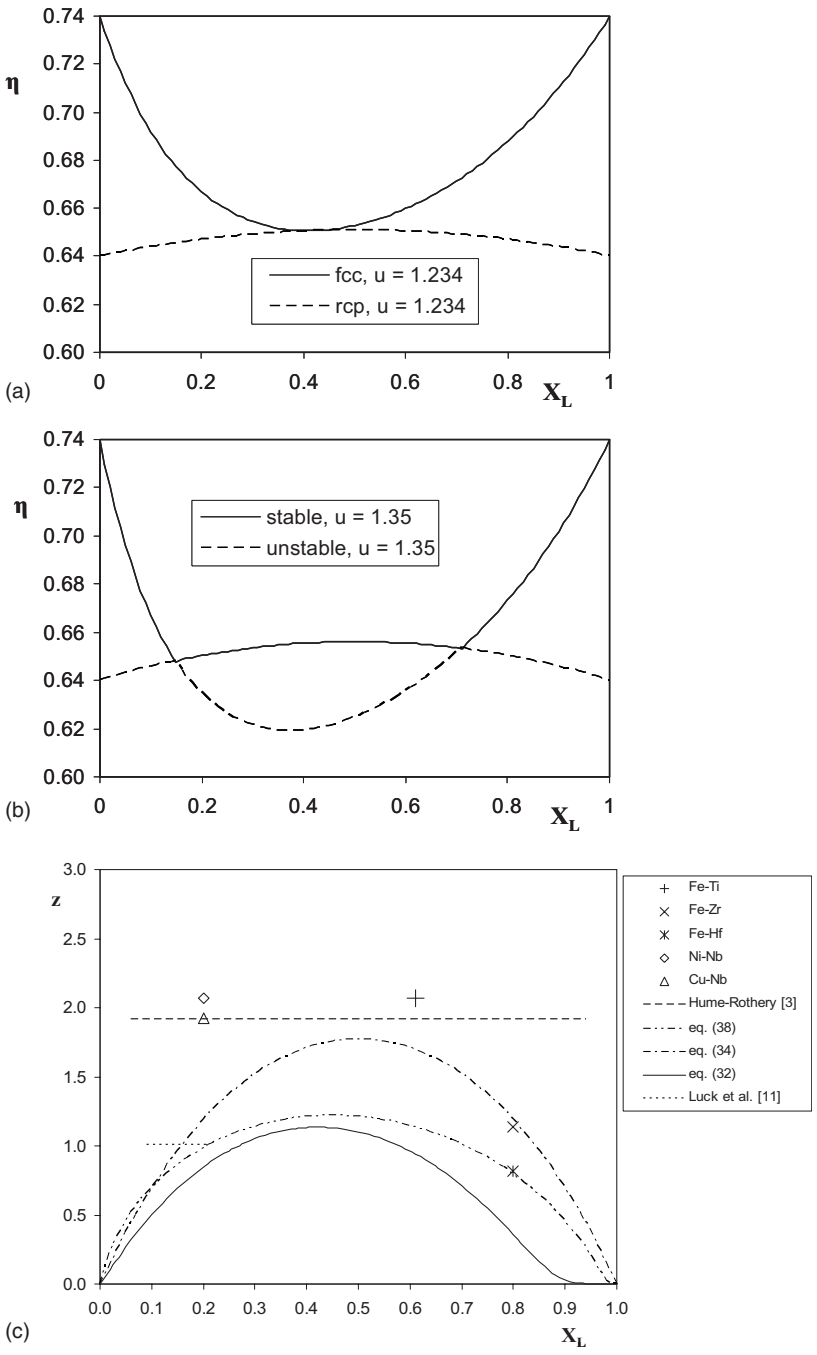

FIG. 6. (a) Packing fraction of bimodal random fcc packing and of bimodal amorphous packing for $u=1.234$ in the range $0 \leq X_L \leq 1$. (b) Packing fraction of bimodal random fcc packing and of bimodal amorphous packing for $u=1.350$ in the range $0 \leq X_L \leq 1$. (c) Packing diagram of bimodal fcc/hcp and rcp packing using the line of crossover (equal packing fraction).

$(0 \leq X_L \leq 1)$ the bcc arrangement has highest packing fraction, hard spheres (and atoms) will favor this arrangement.

In Fig. 7(b) also both packing fractions for $u=1.15$ are depicted. Now we can see that the change in packing fractions is such that there is a compositional range where the binary rcp packing fraction exceeds the bcc packing fraction. This scenario of highest packing is again indicated by the solid line, which indicates the mechanically stable situation of highest packing efficiency. Below $X_{L,\min}$ and above $X_{L,\max}$, bcc is still most preferable, but at intermediate compositions, the space filling ability increases if the bcc structure collapses into a glass and/or amorphous state. Apparently, also here there are compositional regions, depending on the size ratio u, where either bcc or rcp phase are uniquely favored.

To specify the crossover boundary from crystal to glass phase, approximate Eqs. (1) and (21) with $n=6$ are equated, yielding an implicit equation in u and X_L:

$$f_1^{\mathrm{rcp}} + 4\beta f_1^{\mathrm{rcp}}(1-f_1^{\mathrm{rcp}})(1-X_L)X_L\left(\frac{(z+1)^{1/3}-z^{1/3}}{z^{1/3}}\right) = f_1^{\mathrm{bcc}}\left(\frac{X_L+z}{X_L+z+\frac{1}{6}[1-X_L^6-(1-X_L)^6]}\right), \tag{35}$$

whereby Eq. (33) is invoked. In Fig. 7(c) the solution of Eq. (35) is given, whereby z is set out against X_L. This equilibrium line represents the crossover of densest packing

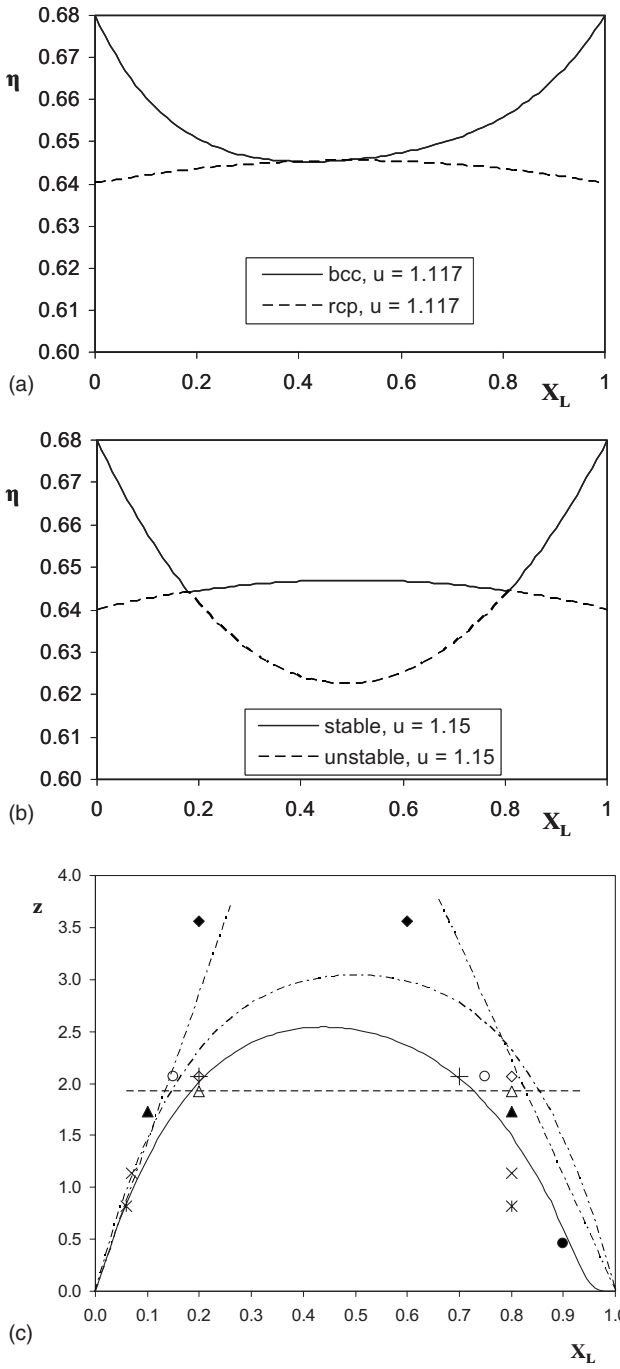

FIG. 7. (a) Packing fraction of bimodal random bcc packing and of bimodal amorphous packing for $u=1.117$ in the range $0 \leq X_L \leq 1$. (b) Packing fraction of bimodal random bcc packing and of bimodal amorphous packing for $u=1.150$ in the range $0 \leq X_L \leq 1$. (c) Packing diagram of bimodal bcc and rcp packing using the line of crossover (equal packing fraction).

between rcp and bcc. For z exceeding this equilibrium, i.e., a smaller size ratio, bcc yields densest packing, below this line rcp yields the densest packing fraction. Note that maximum threshold value of z, $z \approx 2.54$, corresponds to $u=1.117$ [see Eq. (33)], being the value of z above which (value of u below which) a bcc lattice always yields a highest packing fraction, as was seen in Fig. 7(b). Binary spheres with a large size ratio u may, depending on the concentration, form amorphous and/or disordered structures.

For u close to unity, approximate Eqs. (2) and (27) can be equated and combined with Eq. (33), yielding the explicit equation

$$z = (1 - X_L)X_L\left(\frac{\frac{4}{3}\beta f_1^{rcp}(1 - f_1^{rcp}) + f_1^{bcc}\left[1 - \frac{3}{2}(1 - X_L)X_L\right]}{f_1^{bcc} - f_1^{rcp}}\right), \tag{36}$$

which is also included in Fig. 7(c). One can see that this approximate equation matches the full solution quite well in a large range of z and X_L.

In both the fcc-rcp and the bcc-rcp crossover maps one can recognize the threshold size ratio versus terminal composition. For large size ratios, i.e., z tending to zero, there are still $X_{L,min}$ and $X_{L,max}$ below and above which, respectively,

where according to the equations derived here a crystal structure yields optimum packing. These values can be thought of as the terminal solution values pertaining to the concerned size ratio of the spheres.

It should however be kept in mind that the equations derived here become less accurate and are not valid anymore for large u. When $u \geq (\sqrt{2}-1)^{-1}$ (≈ 2.44, i.e., $z < 0.074$) and $u \geq (\sqrt{5/3}-1)^{-1}$ (≈ 3.44, i.e., $z < 0.025$) for fcc and bcc structures, respectively, they are also able to form interstitial solid solutions. These solutions have a higher packing fraction than either the substitutional crystalline or rcp solid solutions studied here. In the next sections the equations derived here are applied to more complicated systems, concerning colloidal suspensions and metal atoms. The borderlines and phase maps based on the hard sphere packing model will be applied to predict their state (amorphous or crystalline).

C. Application to colloidal spheres

Here the results from the previous section are applied to the crystallization of suspended colloidal spheres, which are often used for studying phase transitions. When the concentration of a colloidal suspension increases, a disorder-order transition is frequently observed [11,12]. This corresponds to a transition from a dense fluidlike structure to a crystalline structure. The ability to crystallize depends strongly on the polydispersity, and this has been examined with computer simulations [32], density functional theory [33], a simple model based on Lindemann's melting criterion [34], a basic mean-field model [35], and Monte Carlo simulations [36]. From all studies emerged a critical polydispersity value, σ, above which crystallization to a crystalline structure, mostly fcc, is suppressed. For many particle distributions (such as triangular, rectangular, Schulz) and numerical simulations it followed that this critical degree of polydispersity σ ranges from 5% to 15%. Here, it will be examined if this polydispersity threshold is compatible with the threshold obtained with the hard sphere packing models.

Following the definitions of the previous authors, the polydispersity is defined as the standard deviation of the size distribution divided by the mean diameter, for the here considered discrete bimodal distribution, which consists of $X_S \delta(d-d_S)$ and $X_L \delta(d-d_L)$ with $\delta(x)$ as the Dirac function, it reads

$$\sigma = \frac{[X_L(1-X_L)]^{1/2}(u-1)}{X_L(u-1)+1}. \tag{37}$$

One can see that the polydispersity is promoted by a larger size ratio and when the concentrations of the two components are more equal. Equation (37) can be expressed as

$$\frac{1}{u-1} = \frac{[X_L(1-X_L)]^{1/2} - \sigma X_L}{\sigma}. \tag{38}$$

From this equation, z readily follows, see Eq. (33), which is included in Fig. 6(c) for $\sigma = 10\%$, a value lying in the middle of the range of critical polydispersity values found in the simulation studies addressed above. One can see that the crossover line by the hard sphere packing model is in close quantitative agreement with Eq. (38) in the entire compositional range when this polydispersity value of 10% is adopted. The major difference is, that according to the hard sphere packing model z is proportional to $X_L(1-X_L)$, whereas the referred polydispersity studies yielded a threshold that is proportional to $[X_L(1-X_L)]^{1/2}$. This is due to the definition of the polydispersity, which results in Eq. (37) for the discrete bimodal packing considered here.

The formation of fcc lattices from colloidal suspensions was also studied earlier by Luck *et al.* [11], as discussed already in the previous section. They also observed that for bimodal mixtures of "L32" and "L33," for which $z = 1.006$, see Table II, lattice parameters could be measured for $0 \leq X_L \leq 9.1\%$, but no lattice parameter could be determined for $X_L \geq 21.2\%$, i.e., no crystal structure could then be detected anymore. This implies their crossover concentration is located between 9.1% and 21.2%. This line, $z = 1.006$ and $9\% < X_L < 21\%$, forms the concentration range in which their crossover has taken place, and is drawn in Fig. 6(c) as well. One can see that line is close to the threshold line prescribed by Eq. (32), and actually intersects with the approximate threshold given by Eq. (34). Based on this comparison, one can conclude that both thresholds are not contradicting with the empirical findings [11]. In general, the derived threshold appears to be in line with foregoing numerical and experimental findings in regard to amorphization of colloidal systems.

D. Application to metal alloys

In this section the glass forming ability of metals, which are often modeled as hard sphere systems, is analyzed with the models derived here. The design of alloy compositions with large amorphization (glass forming) ability is an important topic for the bulk production of amorphous metals and metalloids. The amorphization ability of binary alloys is examined using the hard sphere packing descriptions developed here.

The formation and stability of binary alloys upon quenching has been studied intensively in the past. In an early paper Hume-Rothery *et al.* [3] suggested that a maximum atomic size ratio of 14–15 % is favorable for the formation of substitutional solid solutions, and this "amorphization rule" was linked to alloys with atom concentrations exceeding 5%. From various hard sphere simulations it also followed that stable fcc structures are able to form for $u^{-1} > 0.85$ [26,31,33], being compatible with the aforesaid "rule." The resulting threshold line $u = 1.15$ ($z = 1.92$) with $5\% \leq X_L \leq 95\%$ is drawn in Fig. 6(c) as well. This general equation does not account for the concentration of the constituents, which plays a role and should not be ignored.

Egami and Waseda [8] and Liou and Chien [9] investigated experimentally the effect of both atomic size ratio and atomic concentration on amorphization ability. For a number of binary metals, Liou and Chien [9] determined the concentration threshold of amorphous or crystalline phase formation by quenching binary alloys. In Table III their results are summarized (note that the "x" in their formulation corresponds to X_S here, so to $1-X_L$), the results for the fcc and/or hcp hosts are set out in Fig. 6(c).

TABLE III. Compilation of data from quenching experiments by Liou and Chien [9]. Atomic volumes are based on the Goldschmidt atomic radii (12-fold coordination), A and B are the small and large atoms, respectively.

$A_{1-X_L}B_{X_L}$	Structure	Ω_S (Å^3)	Ω_S (Å^3)	Ω_L/Ω_S (u^3)	u	z	$X_{L,min}$	$X_{L,max}$
Fe-Ti	bcc-hcp	8.785	13.036	1.484	1.141	2.066	0.20	0.70
Fe-Zr	bcc-hcp	8.785	16.522	1.881	1.234	1.135	0.07	0.80
Fe-Hf	bcc-hcp	8.785	19.509	2.221	1.305	0.819	0.06	0.80
Fe-Ta	bcc-bcc	8.785	13.856	1.577	1.164	1.732	0.10	0.80
Fe-Mo	bcc-bcc	8.785	11.249	1.281	1.086	3.564	0.20	0.60
B-Fe	rhombo-bcc	2.758	8.785	3.185	1.471	0.458	0.0	0.90
Fe-Nb	bcc-bcc	8.785	13.036	1.484	1.141	2.066	0.15	0.75
Ni-Nb	fcc-bcc	8.785	13.036	1.484	1.141	2.066	0.20	0.80
Cu-Nb	fcc-bcc	8.580	13.036	1.519	1.150	1.926	0.20	0.80

One can see that the measured threshold concentrations are not really compatible with Eq. (32). With the exception of Fe blended Ti, the measured thresholds seem to match Eq. (34). All critical z are higher than predicted by Eq. (32), implying that amorphization takes place at a smaller diameter ratio than predicted with Eq. (32). Considering the work of Liu *et al.* [37], most likely this anomaly can be attributed to the fact that the concerned constituent metals are structurally different. From Arranz *et al.* [38] it follows that the hexagonal Ti can dissolve up to 0.05 at. % Fe only, and that beyond this concentration a Ti-Fe bcc phase is favored. So, both the Fe and Ti rich sides of the packing stability map comprise bcc structures. Accordingly, not only the data of the bcc hosts as listed in Table III, but also all five hcp and/or fcc hosts, are included in Fig. 7(c), which governs the bcc and/or rcp packing stability. The crossover conditions for the Fe-Zr, Fe-Hf, Ni-Nb, and Cu-Nb are all situated closer to the bcc-rcp crossover line than to fcc and/or rcp crossover line; see Figs. 6(c) and 7(c). This conclusion suggests that, likewise, the Fe-Ti alloy, the hcp and/or fcc rich sides (Zr, Hf, Ni, Cu) of the alloys actually adopt a bcc structure, i.e., both the small and large atom rich sides take a bcc structure.

In Fig. 7(c), two empirical fits by Liou and Chien [9],

$$X_{L,min} = 0.07z, \tag{39}$$

$$X_{L,max} = 1 - 0.09z, \tag{40}$$

for the threshold concentrations versus scaled size ratio are also included. These line fits are compatible with their experimental findings. Both lines predict the threshold well near both the small and large atom rich compositions. By equating Eqs. (39) and (40), they derived $z=0.16^{-1}$, representing the value of z where both lines intersect. In view of Eq. (33), they proposed critical $u^3=1.16$ and consequently $u\approx 1.05$, a minimum diameter ratio required for amorphization, which is very small. Egami and Waseda [8] proposed similar equations as Eqs. (39) and (40), only as coefficients the values 0.1 and −0.1 instead of 0.07 and −0.09, respectively, were obtained by fitting [implying that the two lines in Fig. 7(c) would have a more gentle slope]. By equating their threshold lines it follows to achieve amorphization, $z < 0.20^{-1}$, or $u^3 > 1.2$ and consequently $u > 1.06$. Furthermore, likewise in Fig. 6(c), also in Fig. 7(c) the general, concentration independent threshold, $u=1.15$ ($z=1.92$) is included again, based on Hume-Rothery *et al.* [3]. From the crossover lines determined here, the threshold is continuous in the entire compositional range and has a parabolic shape, and the threshold z, and related u, depends on the structure (bcc or fcc and/or hcp). For bcc the maximum crossover z amounts 2.537 and minimum $u=1.117$, and for fcc and/or hcp the maximum $z=1.135$ and minimum $u=1.234$.

From Fig. 7(c) it follows that Eq. (35) and approximate Eq. (36), derived for bcc structures, predicts the empirically observed crossover threshold of the considered alloys remarkably well, especially when it is realized that the present model is solely based on an analytical analysis, without the introduction of a fitting parameter. In the entire compositional range and for many diameter ratios, Eqs. (35) and (36) signal correctly when the quenched alloy favors crystalline or amorphous phase formation. It indicates that "simple" hard sphere models, that ignore many other phenomena involved, but for which no additional adjustable parameter has been introduced nor needed, can be successfully used to assess the behavior of more complicated processes and phenomena.

As said, here the packing diagram of the hard sphere instability model is applied to the glass and/or crystal formation of the alloys listed in Table III. It is known that the atomic diameters are not a true constant, this is a feature ignored by the model. It is known that upon the polymorphic transition from an fcc to a bcc structure, the latter having a 8% lower packing efficiency, the atomic volume decreases in order to maintain a volume and specific density that are almost constant. Actually, the atomic diameters used in Table III are all based on the fcc configuration. In this context, using the lattice data of various salts and alloys, Goldschmidt [39] determined the dependence of atomic radii on structure. For the transformation from fcc to bcc a diameter decrease from 3% was observed. As pointed out by Hume-Rothery *et al.* [3], also the information on monosized sphere packing fraction can be used to assess the diameter adjustment involved with packing fraction adjustment. Assuming invariant total volume and specific density of the material, then it readily follows that

$$d^{\mathrm{bcc}} = \left(\frac{f_1^{\mathrm{bcc}}}{f_1^{\mathrm{fcc}}}\right)^{1/3} d^{\mathrm{fcc}}, \tag{41}$$

substituting $f_1^{\mathrm{fcc}}=2^{1/2}\pi/6$ and $f_1^{\mathrm{bcc}}=3^{1/2}\pi/8$ yields $d^{\mathrm{bcc}}=0.97d^{\mathrm{fcc}}$. So, this packing based approach is compatible with Goldschmidt's rule indeed.

Also upon the transition from crystalline to amorphous phase, the specific density remains practically constant, whereas the packing fraction is reduced, e.g., from monosized fcc to monosized rcp even with 14%. In other words, the observed diameter contraction involved with amorphization represents a polymorphic transition as well.

Actually, the atomic diameters and/or volumes of both constituents in the alloy are reduced. But in the packing models of hard spheres as developed and employed here, it is seen that the *atomic volume ratio* is the relevant parameter in the packing diagram. Applying the hard sphere models, it was assumed *a priori* that the volumes of both concerned atoms expand and/or compress congruently, hence that their diameter ratio remains constant. From the agreement between the present model and empirical amorphization data, as illustrated by Figs. 6(c) and 7(c), it appears that this assumption seems to hold. In a naive way it may perhaps be said that the bonding forces in bimodal crystalline and amorphous states are such that the atomic radii of both constituents are equally affected.

Furthermore, the present hard sphere model is only applicable to alloys when the cooling rate is high, so that polymorphic crossovers between crystalline and glassy phases are possible. At low cooling rates, the organizing of atoms in crystalline phases cannot be suppressed. For Eqs. (7) and (21) to be applicable, a completely random placement of the atoms in the lattice is namely required.

V. CONCLUSION

In the present study the packing fraction of the disordered bimodal cubic structures (fcc, bcc, sc), composed of hard spheres, has been derived. To this end, first a statistical order model for the unit cell volume is presented. The fcc cell volume, resulting from this first-order approach, is illustrated by Fig. 3 [Eq. (14)]. Combined with the mean sphere volume, compact equations for the bimodal packing fraction are obtained in the case of randomly placed bimodal spheres. The predictions of the new unit cell volume model, and its related lattice parameter, are in very good agreement with available empirical data on fcc lattice parameters [11,30], see also Table II. They can, for example, also be used for the further assessments on the state of hard spheres mixtures and metal and/or metalloid alloys. When metal or metalloids are alloyed, the effective lattice parameter is namely the result of geometrical dilatation and other effects, such as electronic contraction. If the actual lattice parameter or distortion parameter of the alloy is specified, which can be found for instance in Pearson [40] and King [41], the present equations for the geometrical expansion enable the quantification of all other remaining effects (e.g. valence and electronegativity).

The derived basic packing fraction equation [Eq. (21)] reveals the opposite trend as observed with rcp, namely a reduced packing fraction upon mixing two sizes of spheres by expansion of the lattice. Thus it appears that the packing faction of binary rcp and the crystalline packing of hard spheres are uniquely characterized by two parameters: the concentration of the two components (actually by one of them, here X_{L} is selected) and the sphere diameter ratio (u). For the fcc structure the scaled packing fraction is governed by Eq. (21) with $n=4$, and its approximation Eqs. (25) and (30). For the bcc structure, Eq. (21) with $n=6$ and Eqs. (26) and (27) hold, and the scaled bimodal packing of the sc structure is governed by Eqs. (21), with $n=8$, and by Eqs. (28) and (29). Whereas for the monosized packing fractions ($u=1$) hold $f_1^{\mathrm{fcc}}>f_1^{\mathrm{bcc}}>f_1^{\mathrm{sc}}$, the effect of size difference has the opposite effect on the scaled bimodal packing fraction: $\eta_{\mathrm{fcc}}/f_1^{\mathrm{fcc}}<\eta_{\mathrm{bcc}}/f_1^{\mathrm{bcc}}<\eta_{\mathrm{sc}}/f_1^{\mathrm{sc}}$ for identical u and X_{L} ($u>1, 0<X_{\mathrm{L}}<1$). Considering the derivation that underlies these expressions for the three lattices of the cubic system (Fig. 2), these scaled packing fractions can also be applied to the other 11 Bravais lattices of the five other crystal systems: triclinic, monoclinic, orthorhombic, hexagonal and/or rhombohedral, and tetragonal.

The gradient β, the gradient in packing fraction on the transition form unimodal to bimodal packing, governed by Eq. (23), follows directly from the bimodal packing equations, and are included in Table I. The values are negative, being in line with packing reduction when spheres of different sizes are combined. In [15] an analytical expression is presented that governs the packing fraction of continuous geometric packings, and that among others contains β and f_1. With the present β values, one could compute the packing fraction of crystalline structures that are composed of spheres with a continuous geometric size distribution as well. In contrast to amorphous packings, that have positive values of β (Table I), these polydisperse crystalline structures will have a packing fraction that is smaller than their monosized version. By combining continuously sized spheres and/or atoms, it is therefore conceivable that an amorphous state is achievable for a diameter width that is larger than possible with using two discrete spheres sizes. The bimodal (discrete) spheres are namely able to form interstitial solutions when the size ratio u exceeds $(\sqrt{2}-1)^{-1}$, $(\sqrt{5/3}-1)^{-1}$, and $(\sqrt{3}-1)^{-1}$ for fcc, bcc, and sc structures, respectively, being more favorable than the amorphous state (from a packing point of view) of bimodal spheres.

Next, by combining the packing fraction of binary rcp and the crystalline structures, the mode of highest packing efficiency for binary mixtures is obtained. It is confirmed that the reduction (crystalline) and increase (rcp) in packing fraction can be such that the packing fraction of rcp phase exceeds that of the regular structures, i.e., from a topological point of view the random (amorphous) state becomes more favorable [42]. For the fcc and bcc structures, on space-filling grounds and/or arguments, maps of closest packing mode are established that govern the transition to rcp [Figs. 6(c) and 7(c)]. This amorphization transition threshold is governed by a single implicit algebraic equation, comprising the sphere diameter ratio and concentration only. As small diameter ratios are relevant only (at large diameter ratios interstitial solid solutions become feasible), simple and con-

venient explicit approximate equations, viz. Eqs. (34) and (36), are presented that match the exact solutions well.

Finally, the theoretical results are applied to two relevant crystallization and/or amorphization processes. The first process concerns the crystallization of colloidal spheres. The other process concerns the amorphization of quenched binary alloys of metals and metalloids, comprising a large variation on diameter ratios and composition. Both comparisons yield good agreement, confirming the usefulness of the derived compact equations, which are based on a geometrical consideration of packing only, and without the introduction of an adjustable parameter.

In reality the atomic volumes of the alloy constituents are different in amorphous and crystalline states, due to different packing fraction and, at the same time, a relatively constant specific density. But from the present results one may furthermore conclude that this atomic volume expansion and/or contraction affects both constituents congruently, so that both the rcp and crystalline bimodal packing equations that contain the atomic diameter ratio u, can be directly equated, although the absolute volumes of the atoms and/or spheres are not identical.

Another result is that, for formation of an fcc structure, the polydispersity of the spheres should be smaller than about 10%, being compatible with the value obtained with other types of studies. Furthermore, for the formation of crystalline fcc and/or hcp and bcc substitutional binary alloys, or to avoid the possibility of amorphization in the entire composition range, the diameter ratio should be smaller than about 1.23 and 1.12, respectively. Moreover, on applying the present model to alloys of metals and/or metalloids that are structurally different, it should be realized that some hcp and/or fcc hosts seem to favor a bcc structure when alloyed with a bcc structured constituent. Hence, in this case the bcc crossover map prevails in the entire compositional range [Fig. 7(c)]. Probably one could also use the information on crossover behavior conversely: depending on whether the alloy crossover obeys the lines of Figs. 6(c) and 7(c), one could be able to assess the structure of the host rich side, which may be different from the structure of the pure host.

Concluding, one can say that the results of this study are a strong support for the applicability and validity of "simple" noninteracting hard sphere packing models to describe the state of more complex materials and phenomena.

ACKNOWLEDGMENT

The author acknowledges the assistance of G. Hüsken with the drawing of Figs. 1 and 2, and the numerical solution of Eqs. (32) and (35).

[1] J. P. Hansen and I. R. McDonald, *Theory of Simple Liquids* (Academic, New York, 1976).
[2] E. Parthé, Z. Kristallogr. **115**, 52 (1961); *Crystal Chemistry of Tetrahedral Structures* (Gordon and Breach, New York, 1964).
[3] W. Hume-Rothery, G. W. Mabbott, and K. M. Channel-Evans, Philos. Trans. R. Soc. London, Ser. A **233**, 1 (1934); W. Hume-Rothery, R. E. Smallman, and C. W. Haworth, *The Structure of Metals and Alloys*, 5th ed. (revised) (Institute of Metals, London, 1969).
[4] L. S. Darken and R. W. Gurry, *Physical Chemistry of Metals* (McGraw-Hill, New York, 1953).
[5] J. R. Chelikowsky, Phys. Rev. B **19**, 686 (1979).
[6] A. R. Miedema, P. F. de Châtel, and F. R. de Boer, Physica B & C **100**, 1 (1980).
[7] B. Rauschenbach and K. Hohmuth, Phys. Status Solidi A **72**, 667 (1982) (in German).
[8] T. Egami and Y. Waseda, J. Non-Cryst. Solids **64**, 113 (1984).
[9] S. H. Liou and C. L. Chien, Phys. Rev. B **35**, 2443 (1987).
[10] O. N. Senkov and D. B. Miracle, Mater. Res. Bull. **36**, 2183 (2001).
[11] W. Luck, M. Klier, and H. Wesslau, Ber. Bunsenges. Phys. Chem. **67**, 75 (1963) (in German).
[12] P. N. Pusey and W. van Megen, Nature (London) **320**, 340 (1986).
[13] C. C. Furnas, Department of Commerce, Bureau of Mines, Report of Investigation Serial No. 2894, 1928 (unpublished); C. C. Furnas, Bull U.S. Bureau Mines **307**, 74 (1929).
[14] P. C. Mangelsdorf and E. L. Washington, Nature (London) **187**, 930 (1960).
[15] H. J. H. Brouwers, Phys. Rev. E **74**, 031309 (2006); **74**, 069901(E) (2006).
[16] G. D. Scott, Nature (London) **188**, 908 (1960); G. D. Scott and D. M. Kilgour, Br. J. Appl. Phys. **2**, 863 (1969).
[17] For small size ratio $c_S=X_S$ and $c_L=X_L$, i.e., volume factions c and mole fractions X, are practically equal.
[18] A. R. Kansal, S. Torquato, and F. H. Stillinger, J. Chem. Phys. **117**, 8212 (2002).
[19] R. K. McGeary, J. Am. Ceram. Soc. **44**, 513 (1961).
[20] A. S. Clarke and J. D. Wiley, Phys. Rev. B **35**, 7350 (1987).
[21] J. W. Retgers, Z. Phys. Chem., Stoechiom. Verwandtschaftsl. **3**, 497 (1889) (in German).
[22] E. Zen, Am. Mineral. **41**, 523 (1956).
[23] A. E. Van Arkel and J. Basart, Z. Kristallogr. **68**, 475 (1928) (in German).
[24] L. Vegard, Z. Phys. **5**, 17 (1921) (in German).
[25] P. Jalali and M. Li, Phys. Rev. B **71**, 014206 (2005).
[26] A. R. Denton and N. W. Ashcroft, Phys. Rev. A **42**, 7312 (1990).
[27] A. R. Denton (private communication).
[28] Their bimodal packing equation reads $\eta_{fcc}/f_1^{fcc}=[X_L(u^3-1)+1]/u^3$.
[29] W. Luck (private communication).
[30] H. E. v. Steinwehr, Z. Kristallogr. **125**, 360 (1967) (in German).
[31] W. G. T. Kranendonk and D. Frenkel, Mol. Phys. **72**, 679 (1991); **72**, 715 (1991).
[32] E. Dickinson and R. Parker, J. Phys. (France) Lett. **46**, L229 (1985).
[33] J. L. Barrat, M. Baus, and J. P. Hansen, Phys. Rev. Lett. **56**, 1063 (1986); J. Phys. C **20**, 1413 (1987).

[34] P. N. Pusey, J. Phys. (Paris) **48**, 709 (1987).
[35] P. Bartlett and P. B. Warren, Phys. Rev. Lett. **82**, 1979 (1999).
[36] D. A. Kofke and P. G. Bolhuis, Phys. Rev. E **59**, 618 (1999).
[37] B. X. Liu, W. L. Johnson, and M. A. Nicolet, Appl. Phys. Lett. **42**, 45 (1983).
[38] M. A. Arranz, T. Muñoz, and J. M. Riveiro, Phys. Rev. B **66**, 144417 (2002).
[39] V. M. Goldschmidt, Z. Phys. Chem., Stoechiom. Verwandtschaftsl. **133**, 397 (1928) (in German).
[40] W. B. Pearson, *Lattice Spacings and Structure of Metals and Alloys*, (Pergamon, New York, 1958), Vols. 1 and 2.
[41] H. W. King, J. Mater. Sci. **1**, 79 (1966).
[42] Also known as Laves' Principle: The most stable structure for a solid is one in which the most efficient use is made of space.
[43] M. Iannella, B.Eng. thesis, University of Wollongong, Wollongong, Australia, 1985.
[44] A. B. Yu, N. Standish, and A. McLean, J. Am. Ceram. Soc. **76**, 2813 (1993).
[45] A. N. Patankar and G. Mandal, Trans. J. Br. Ceram. Soc. **79**, 59 (1980).
[46] A. H. M. Andreasen and J. Andersen, Kolloid-Z. **50**, 217 (1930) (in German).